








Article

Ferro-ferri-katophorite, a new clinoamphibole from the silicocarbonatite dykes in Sierra de Maz, La Rioja, Argentina

Fernando Colombo^{1,2,3*} , Jordi Rius¹ , Elies Molins¹, Héctor Biglia², Miguel Á. Galliski⁴ ,
María Florencia Márquez-Zavalía^{4,5}, Edgardo G. A. Baldo³  and Agustín Kriscoutzky^{2,6} 

¹Institut de Ciència de Materials de Barcelona (ICMAB-CSIC), Campus UAB, 08193 Bellaterra, Spain; ²Universidad Nacional de Córdoba, Facultad de Ciencias Exactas, Físicas y Naturales, Cátedra de Mineralogía, Vélez Sarsfield 1611 (X5016GCA) Córdoba, Argentina; ³CONICET, CICTERRA, Vélez Sarsfield 1611 (X5016GCA) Córdoba, Argentina; ⁴IANIGLA, CCT-MENDOZA CONICET, Avda. Ruiz Leal s/n, Parque Gral. San Martín, C.C. 330, (5500) Mendoza, Argentina; ⁵Mineralogía y Petrología, FAD, Universidad Nacional de Cuyo, Centro Universitario (5502) Mendoza, Argentina; and ⁶School of Physical Sciences, University of Arkansas at Little Rock, 2801 S. University Ave. Little Rock AR – 72204 (ETAS 329L), USA

Abstract

Ferro-ferri-katophorite (IMA2016–008), ideally $\text{Na}(\text{NaCa})(\text{Fe}_4^{2+}\text{Fe}^{3+})(\text{Si}_7\text{Al})\text{O}_{22}(\text{OH})_2$, was found as xenocrysts up to 3 cm long and replacement rims around aegirine–augite in silicocarbonatite dykes cropping out in the Sierra de Maz, La Rioja province, NW Argentina. Ferro-ferri-katophorite is black and has vitreous lustre and a pale green streak. The new mineral is brittle, with perfect {110} cleavage and has a Mohs hardness of 6. The measured density is 3.32(1) g/cm³. In plane-polarised light it is strongly pleochroic, X = light greenish brown, Y = dark greyish brown and Z = dark greyish olive green. Absorption (very strong) is Z > Y > X. The orientation is: Z || b, and X forms a small angle with [001]. Ferro-ferri-katophorite is biaxial (–), with $\alpha = 1.688(3)$, $\beta = 1.697(3)$, $\gamma = 1.698(3)$ and 2V (calc) = 36.7°. It is monoclinic, space group C2/m, $a = 9.8270(7)$, $b = 18.0300(8)$, $c = 5.316(4)$ Å, $\beta = 104.626(4)^\circ$, $V = 911.4(6)$ Å³ and Z = 2. The strongest five lines in the powder X-ray diffraction pattern [d in Å (I)(hkl)] are: 8.416(100)(110), 3.135(50)(310), 2.815(26)(330), 2.720(18)(151) and 1.4422(15)(661). The chemical composition is SiO_2 43.08, TiO_2 2.76, ZrO_2 0.15, Al_2O_3 8.76, V_2O_5 0.07, Fe_2O_3 9.28, FeO 13.85, MnO 0.43, MgO 6.88, CaO 6.58, ZnO 0.06, Na_2O 5.55, K_2O 1.18, Cl 0.01, H_2O calc 1.36, total 99.95 wt.%. The formula unit (confirmed by single-crystal structural analysis) is $(\text{Na}_{0.74}\text{K}_{0.23})_{\Sigma 0.97}(\text{Ca}_{1.08}\text{Na}_{0.91}\text{Mn}_{0.01})_{\Sigma 2.00}(\text{Fe}_{1.78}\text{Mg}_{1.57}\text{Fe}_{1.07}\text{Tl}_{0.32}\text{Al}_{0.19}\text{Mn}_{0.04}\text{Zr}_{0.01}\text{V}_{0.01}\text{Zn}_{0.01})_{\Sigma 5.00}(\text{Si}_{6.61}\text{Al}_{1.39})_{\Sigma 8.00}\text{O}_{22}(\text{OH}_{1.59}\text{O}_{0.61})_{\Sigma 2.00}$. Aluminium is strongly ordered at the T(1) site. Ferro-ferri-katophorite is the 9th species carrying the katophorite root name and is related to katophorite by the $\text{Fe}^{2+} + \text{Fe}^{3+} \rightarrow \text{Mg}^{2+} + \text{Al}^{3+}$ substitution. Type material was deposited at the Museo de Mineralogía “Stelzner”, Universidad Nacional de Córdoba, Argentina, under catalogue number MS003341.

Keywords: sodium-calcium amphibole, silicocarbonatite, new mineral species, Mössbauer spectroscopy, single-crystal structural refinement, La Rioja, Argentina

(Received 30 November 2021; accepted 30 December 2022; Accepted Manuscript published online: 19 January 2023; Associate Editor: Giancarlo Della Ventura)

Introduction

In the eastern flank of the Sierra de Maz, La Rioja Province, NW Argentina (29.23°S, 68.35°W) there is a deformed silicocarbonatite–nepheline syenite complex which, unlike other carbonatites known in western South America, is the only known body of Neoproterozoic age (*ca.* 570 Ma, SHRIMP U–Pb in zircon, Casquet *et al.*, 2008a). Silicocarbonatite (SiO₂ wt.% ranging from 17.16 to 28.92, Biglia 2015) is the main lithological type, with syenite (with or without nepheline) occurring as metre-sized blocks and smaller rounded inclusions within the carbonatite. Together, the subparallel dykes define a system that extends in a north–south direction for ~4 km, with a maximum width of ~120 m, hosted by biotite–garnet ± hornblende gneisses, orthoamphibolites,

metagabbros and local meta-peridotites. They are located within the Maz Central Domain, which records two main metamorphic episodes, one during the Neoproterozoic (1.2 Ga) and another one at 431 ± 40 Ma (Casquet *et al.*, 2008b).

Xenocrysts of aegirine–augite, amphibole and biotite are widespread as irregular masses scattered in the medium-grained biotite–plagioclase silicocarbonatite (Fig. 1a). With the exception of those found in a small dyke that runs parallel to the main system, xenocrysts display markedly Fe-dominant compositions, which is unusual for ferromagnesian silicates in carbonatites.

‘Katophorite amphibole’ (ferro-ferri-katophorite according to the electron microprobe chemical data, but not specifically identified as such) was found by C. Galindo and reported by Casquet *et al.* (2008a) as a replacement product of aegirine–augite that forms enclaves composed of albite, magnetite, ferroan calcite and amphibole. A later systematic survey, undertaken to document the chemical variability and textural relationships among ferromagnesian silicates, showed that the new amphibole is rather widespread, both as reaction rims and as xenocrysts. The new

*Author for correspondence: Fernando Colombo, Email: fosfatos@yahoo.com.ar

Cite this article: Colombo F., Rius J., Molins E., Biglia H., Galliski M.Á., Márquez-Zavalía M.F., Baldo E.G.A. and Kriscoutzky A. (2023) Ferro-ferri-katophorite, a new clinoamphibole from the silicocarbonatite dykes in Sierra de Maz, La Rioja, Argentina. *Mineralogical Magazine* 87, 324–330. <https://doi.org/10.1180/mgm.2023.2>

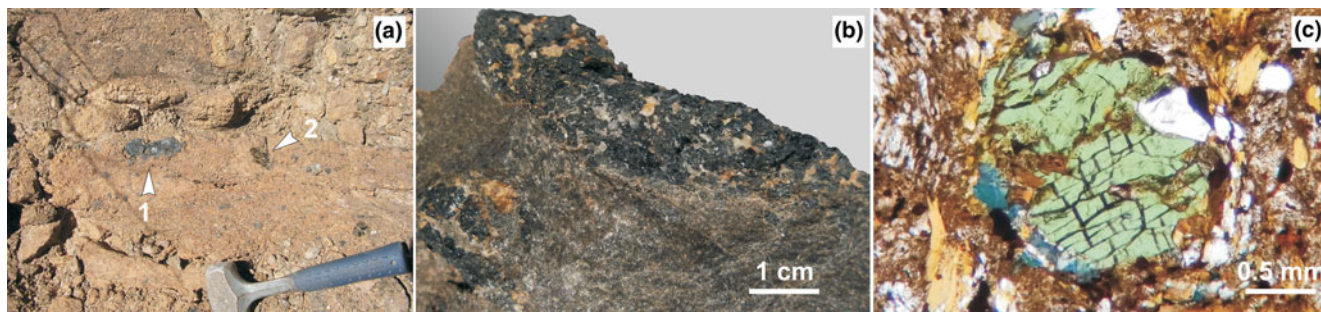


Fig. 1. (a) Masses of aegirine-augite and amphibole (number 1) and biotite (number 2) scattered in silicocarbonatite outcrop; (b) aggregate of granular ferro-ferri-katophorite associated with calcite and albite, in silicocarbonatite (FC collection #02257); (c) photomicrograph under plane polarised light, showing the basal section of an aegirine-augite crystal (green) replaced along the rims by a granular aggregate of ferro-ferri-katophorite (blue), in a silicocarbonatite matrix.

species and name (symbol Ffktf) has been approved by the Commission on New Minerals, Nomenclature and Classification of the International Mineralogical Association (IMA2016-008, Colombo *et al.*, 2016). The name conforms to the current nomenclature scheme for amphiboles of Hawthorne *et al.* (2012). Type material (fragment of the holotype) has been deposited in the collection of the Museo de Mineralogía “Dr. Alfred Stelzner”, Universidad Nacional de Córdoba (Argentina), under catalogue number MS003341.

Occurrence

Ferro-ferri-katophorite occurs as granular masses (Fig. 1b) or as replacement rims around aegirine-augite crystals (Fig. 1c). In the first case individual crystals may reach 3 cm and show the {110} monoclinic prism elongated along [001], with ragged terminations. They are poikilitic, with inclusions of albite and calcite. When ferro-ferri-katophorite occurs as a replacement of aegirine-augite, it forms polycrystalline rims showing lobate contacts against the clinopyroxene. Crystals have an approximately parallel orientation, as they display similar colours under parallel polarised light.

All of the properties and the chemical data reported in this paper were measured on a single crystal of ferro-ferri-katophorite.

Physical and optical properties

Macroscopically, ferro-ferri-katophorite is black and opaque, with vitreous lustre and a pale greyish green streak. It does not fluoresce under ultraviolet radiation (either long- or shortwave). Grains display the typical perfect {110} cleavage of amphiboles. No twinning was observed. The mineral is brittle, with irregular or splintery fracture. Mohs hardness is 6.0. The measured density is 3.32(1) g/cm³ (determined by immersion in toluene, $n = 2$), while the calculated value is 3.358 g/cm³ based on the empirical formula using single-crystal unit-cell parameters.

Under the polarising microscope, ferro-ferri-katophorite shows a very strong absorption and is transparent only in very thin fragments. Optical properties were determined using white light and calibrated immersion oils. Ferro-ferri-katophorite is biaxial (-), with $\alpha = 1.688(3)$, $\beta = 1.697(3)$, $\gamma = 1.698(3)$ and $2V_{\text{calc}} = 36.7^\circ$. The observed $2V$ was small, but could not be measured accurately because of indistinct interference figures and very strong absorption. It displays very strong parallel dispersion, with $r > v$. The orientation is: $Z \parallel b$, and X forms a small angle with [001]. Pleochroism is very strong, with X = light greenish

brown, Y = dark greyish brown and Z = dark greyish olive green. Absorption is $Z > Y > X$. It should be noted that amphibole (identified as ferro-ferri-katophorite by electron microprobe analyses) rimming clinopyroxene may display pleochroism with bluish colours.

The compatibility index $1 - (K_p/K_c)$ is 0.030 (excellent) for the empirical formula using the density derived from the single-crystal unit cell, and 0.019 (superior) for the empirical formula using the density derived from powder X-ray diffraction data.

Chemical composition

Electron microprobe analysis

Ferro-ferri-katophorite was analysed using wavelength dispersive spectroscopy on a JEOL JXA-28230 electron microprobe (LAMARX-Universidad Nacional de Córdoba, Argentina) operated at an accelerating voltage of 15 kV and a beam current of 20 nA. The beam was defocused to 10 μm . We measured $K\alpha$ lines, except for Zr ($L\alpha$). An empirical Ti-V overlap correction was applied. Data reduction was made with ZAF, as implemented by the JEOL software. The chemical composition of the type specimen appears in Table 1, along with standards and monochromator crystals. No zoning was detected using back-scattered electron images. An average of the composition of replacement rims around aegirine-augite (taken from Casquet *et al.*, 2008a) is also listed for comparison. The calculated structural formulae appear in Table 2, column 1 (for the type specimen) and column 5 (for the rims).

H₂O and O²⁻ contents were calculated based on a combination of results from the electron microprobe (EMP) and Mössbauer analyses, and the crystal structure refinement (as there is a relationship between Ti at the M(1) site and O²⁻ content). For the rims around aegirine-augite, the information is more limited, as neither Mössbauer spectroscopy nor a structural study could be performed. In that case the formula was calculated under the assumption that per each Ti atom that enters at the M(1) position replacing a divalent cation, two protons are lost.

Chromium (detection limit 120 ppm, LIFH, chromite standard) was also sought but not found. A single analysis shows an F content of 0.13 wt.%; however, the average value is below the detection limit for this element (670 ppm, TAP, fluorapatite standard). For the calculation of average values, analyses below the detection limit were considered as 0.00.

Oxygen (as O²⁻) at the O3 site was calculated by charge balance, with (OH)⁻ obtained as (2-O²⁻-F⁻-Cl⁻) atoms per formula

Table 1. Chemical composition of ferro-ferri-katophorite (single crystal data from this work, and rims around aegirine–augite from Casquet *et al.*, 2008a).

Constituent	Single crystal (<i>n</i> = 7)			Probe standard/ crystal	Rims around aegirine–augite (<i>n</i> = 5)
	Wt.%	Range	S.D.		Casquet <i>et al.</i> (2008a)
SiO ₂	43.08	42.45–43.33	0.33	kaersutite/TAP	44.03
TiO ₂	2.76	2.52–3.10	0.22	ilmenite/LIF	1.27
ZrO ₂	0.15	0.10–0.20	0.04	Y-doped ZrO ₂ / PETH	
Al ₂ O ₃	8.76	8.56–8.92	0.16	orthoclase/TAP	7.08
FeO (total)	[22.21]	22.05–22.44	0.17	fayalite/LIFH	22.78
Fe ₂ O ₃ *	9.28				
FeO*	13.85				
MnO	0.43	0.37–0.48	0.04	rhodonite/LIFH	0.53
MgO	6.88	6.84–7.08	0.11	kaersutite/TAP	7.26
CaO	6.58	6.52–6.64	0.05	kaersutite/PETJ	6.66
ZnO	0.05	<0.04–0.13	0.04	ZnO/LIFH	
V ₂ O ₃	0.07	<0.05–0.13	0.05	ScVO ₄ /LIF	
Na ₂ O	5.55	5.38–5.65	0.09	albite/TAP	5.29
K ₂ O	1.18	1.10–1.22	0.04	orthoclase/PETJ	1.06
Cl	0.01	<0.01–0.02	<0.01	sodalite/PETJ	
H ₂ O _{calc}	1.36				
Total	99.95				

S.D. – standard deviation

*Total Fe expressed as Fe₂O₃ and FeO based on the Mössbauer spectroscopy results. O≡Cl = 0.002 wt.%, eliminated by rounding off.

unit (apfu). The empirical formula of the single crystal is: (Na_{0.74}K_{0.23})_{Σ0.97}(Ca_{1.08}Na_{0.91}Mn_{0.01})_{Σ2.00}(Fe²⁺_{1.78}Mg_{1.57}Fe³⁺_{1.07}Ti⁴⁺_{0.32}Al_{0.19}Mn²⁺_{0.04}Zr_{0.01}V³⁺_{0.01}Zn_{0.01})_{Σ5.00}(Si_{6.61}Al_{1.39})_{Σ8.00}O₂₂(OH_{1.59}O_{0.61})_{Σ2.00}. The amount of Cl is above the electron microprobe detection limit, however it is only equivalent to 0.002 Cl apfu and is thus eliminated by rounding off. The ideal formula is Na(NaCa)(Fe²⁺Fe³⁺)(Si₇Al)O₂₂(OH)₂, which requires (in wt.%) SiO₂ 43.14, Al₂O₃ 5.23, Fe₂O₃ 8.19, FeO 29.48, CaO 5.75, Na₂O 6.36, H₂O 1.85, total 100.00%.

Mössbauer spectroscopy

The Mössbauer spectrum of a powdered sample was acquired in transmission geometry at 298 K using a conventional transmission Mössbauer spectrometer with a ⁵⁷Co/Rh source. The spectrometer was calibrated with the room-temperature spectrum of α-Fe. The program package *Fit;o* (Hjellum and Madsen 2009) was used to fit the spectrum using doublets (Fig. 2). Both peaks of each doublet were constrained to have the same area and same width. The results are shown in Table 3, where the distribution of Fe²⁺ and Fe³⁺ obtained by single-crystal structural refinement has been reported for comparison.

Crystallography

Powder X-ray diffraction

Powder X-ray diffraction data were recorded using a Siemens D-5000 diffractometer in Bragg-Brentano geometry using CuKα₁₊₂ radiation. Observed *d* values and intensities were derived by full-profile fitting using the *FullProf* software (Rodríguez-Carvajal, 2001). Observed intensities are affected by preferred orientation due to the perfect {110} cleavage. The strongest five lines in the powder X-ray diffraction pattern [*d* in Å (*hkl*)] are: 8.416(100)(110), 3.135(50)(310), 2.815(26)(330), 2.720

Table 2. Crystal-chemical formulae of ferro-ferri-katophorite calculated according to different normalisation schemes. Average of rim compositions taken from Casquet *et al.* (2008a)*.

Norm. scheme:	Single crystal (Fe ²⁺ /Fe ³⁺ ratio by Mössbauer spectroscopy)	Single crystal FeO _{total} , no deprotonation	Single crystal FeO _{total} , no deprotonation	Single crystal FeO _{total} , O ₀₃ = 2Ti	Rim FeO _{total} , O ₀₃ = 2Ti
	Based on SREF	[1]	[2]	[3]	[1]
T sites					
Si	6.610	6.610	6.602	6.613	6.860
Al	1.390	1.390	1.398	1.387	1.140
ΣT	8.000	8.000	8.000	8.000	8.000
C sites					
Al	0.193	0.194	0.183	0.197	0.160
Ti	0.318	0.318	0.318	0.318	0.149
Zr	0.011	0.011	0.011	0.011	
V	0.006	0.008	0.008	0.008	
Fe ³⁺	1.072	0.452	0.514	1.072	0.884
Fe ²⁺	1.778	2.397	2.331	1.779	2.084
Mn	0.043	0.038	0.056	0.033	0.037
Mg	1.574	1.574	1.572	1.574	1.686
Zn	0.006	0.007	0.007	0.007	
ΣC	5.000	4.999	5.000	4.999	5.000
B sites					
Mn	0.013	0.017	0.000	0.022	0.033
Ca	1.081	1.081	1.080	1.081	1.112
Na	0.906	0.902	0.920	0.896	0.856
ΣB	2.000	2.000	2.000	1.999	2.001
A site					
Na	0.743	0.748	0.728	0.754	0.742
K	0.230	0.230	0.230	0.230	0.211
ΣA	0.974	0.978	0.958	0.984	0.953
W site					
O in O3	0.606	0.000	0.000	0.637	0.298
Cl	0.003	0.003	0.003	0.003	
OH	1.391	1.997	1.997	1.360	1.702
ΣW	2.000	2.000	2.000	2.000	2.000
H ₂ O _{calc}	1.36	1.95	1.96	1.33	1.67
Fe ₂ O ₃	9.28	3.92	4.46	9.28	7.54
FeO	13.85	18.68	18.19	13.86	15.99
Total	99.95	100.04	100.05	99.95	98.39

*Blank: not measured. Normalisation procedures used for formula, as described in Hawthorne *et al.* (2012): [1] average between Si+Ti+Zr+Al+Fe+Mn+Mg+V+Zn = 13 apfu and Σcations = 16 apfu; [2] Si+Ti+Zr+Al+Fe+Mn+Mg+V+Zn = 13 apfu; [3] per 24 (O,OH,Cl).

(18)(151) and 1.4422(15)($\bar{6}61$). The complete dataset (in Å for CuKα₁, Table S1), along with the calculated pattern, has been deposited with the Principal Editors of *Mineralogical Magazine* and is available as Supplementary material. Unit cell parameters measured from powder X-ray diffraction data are *a* = 9.8697(5), *b* = 18.094(1), *c* = 5.3320(4) Å, β = 104.603(4)° and *V* = 921.4(1) Å³.

Single-crystal structure refinement

Data collection and refinement details for the single-crystal structural refinement (SREF) are given in Table 4. Intensities were corrected for Lorentz and polarisation effects. The structure was refined to *R*₁ = 2.77% for 1064 reflections with *I* > 2σ(*I*) using *SHELXL* (Sheldrick 2008), starting from the atomic coordinates of katophorite (sample A7) published by Hawthorne *et al.* (1996). We used ionised atom scattering curves for all atoms, except for H (neutral) and Si, where neutral *vs.* ionised curves were applied (*cf.* Hawthorne *et al.*, 1995). The H atom was located

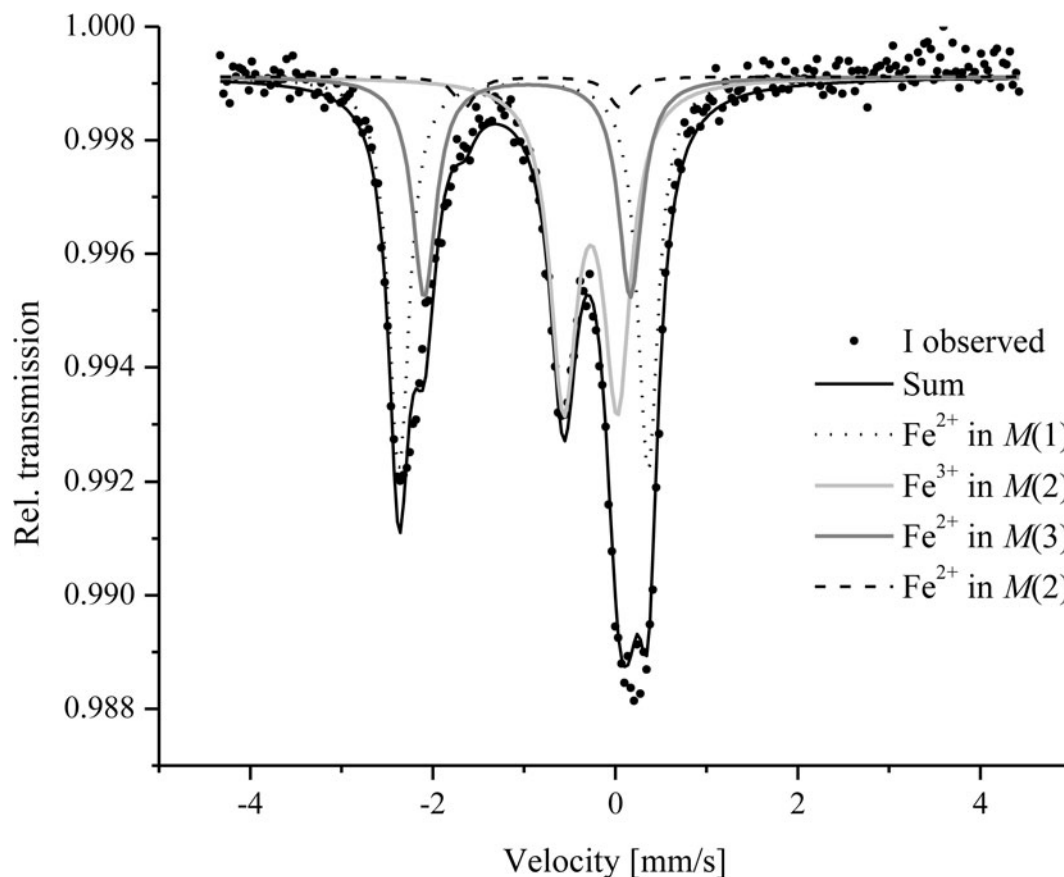


Fig. 2. Mössbauer spectrum of ferro-ferri-katophorite.

by Fourier synthesis; its U_{eq} was constrained to be 1.2 times the U_{eq} of O(3).

Atomic coordinates and atomic displacement parameters (ADP) are listed in Table 5, whereas selected bond lengths appear in Table 6.

Crystal structure and site populations

Site populations calculated on the basis of EMP, Mössbauer spectroscopy and SREF analyses are reported in Table 7.

The $\langle T(2)\text{-O} \rangle$ distance, 1.627 Å, is very short and suggests that no Al occurs at this site; $T(2)$ seems to be fully occupied by Si.

The application of the relationship $T(1)\text{Al} = 32.17 \langle T(1)\text{-O} \rangle - 52.12$, proposed by Hawthorne and Oberti (2007), gives $T(1)\text{Al} = 1.14$ apfu, lower than the 1.40 Al apfu necessary to completely fill the site; nevertheless, the 1.40 value is well within the general

trend shown by Hawthorne and Oberti (2007, their figure 17). Other cations that could occupy tetrahedral sites in amphiboles are Fe^{3+} and Ti^{4+} . However, no fourfold-coordinated Fe^{3+} was detected by Mössbauer spectroscopy. Titanium has been shown to order at the $T(2)$ site, where it causes an increase of $\langle T(2)\text{-O} \rangle$ distance and of the mean atomic number (Oberti *et al.*, 1992); none of these features are present in the sample of ferro-ferri-katophorite studied. Therefore, we conclude that the $T(1)$ site is only occupied by Si and Al, and that this last element is strongly ordered at this site.

Atomic populations in the octahedral $M(1)$, $M(2)$ and $M(3)$ sites were assigned taking into account the refined site-scattering values and $\langle M\text{-O} \rangle$ distances. Calculated distances were based on the values typical for each element as given by Hawthorne (1983, table 28). When no values were available (for Zr, Zn and V^{3+} , all of them present in trace amounts), they were calculated from Shannon (1976). They were assigned to the $M(2)$ site based on the results obtained by Oberti *et al.* (2000) (for Zr) and Hawthorne *et al.* (1993) (Zn). Nevertheless, their assignments remain tentative because of their very low concentration in ferro-ferri-katophorite.

The $M(4)$ site was modelled as a split site [$M(4) + M(4')$], with full occupancy; a small amount of Mn^{2+} was assigned to the $M(4')$ site. Oberti and Ghose (1993) mentioned that the $M(4')$ site has a distorted [6+2] coordination, and can host divalent cations more suitably than the $M(4)$ site.

As in other amphiboles belonging to the sodium–calcium group, alkalis are distributed over two subsites [$A(m)$ and $A(2)$] within the A cavity (Hawthorne *et al.*, 1996). The large ADP

Table 3. Parameters and Fe distribution obtained from the Mössbauer spectrum.

Doublet	Half-band width	Quadrupole splitting	Isomer shift	Area (%)	Assignment	%Fe (SREF)
1	0.27	2.371	-1.005	36.23	Fe^{2+} in $M(1)$	32.68
2	0.36	0.589	-0.270	37.66	Fe^{3+} in $M(2)$	42.62
3	0.28	1.693	-0.800	2.91	Fe^{2+} in $M(2)$	0.99
4	0.31	2.258	-0.963	23.20	Fe^{2+} in $M(3)$	23.71

SREF: single-crystal structural refinement.

Table 4. Details of data collection and structural refinement.

Crystal data	
Ideal formula	Na(NaCa)(Fe ₄ ²⁺ Fe ³⁺)(Si ₇ Al)O ₂₂ (OH) ₂
Empirical formula from the refinement	K _{0.23} Na _{1.62} Ca _{1.10} Fe _{2.87} Mg _{1.67} Ti _{0.32} Al _{1.55} Si _{6.61} H _{1.40} O ₂₄
Crystal dimensions (mm)	0.20 × 0.08 × 0.08
Crystal system, space group	Monoclinic, C2/m (#12)
Temperature (K)	293(2)
a, b, c (Å)	9.8270(7), 18.0300(8), 5.316(4)
β (°)	104.626(4)
V (Å ³)	911.4(6)
Z	2
Calculated density (g cm ⁻³)	3.344
μ (mm ⁻¹)	7.648
F (000)	889
Data collection	
Crystal description	Prismatic fragment bound by cleavage planes
Instrument	Nonius CAD4 with point detector
Radiation type, wavelength (Å)	MoKα, 0.70926
θ range (°)	2.26 to 29.09
Absorption correction	DIFABS (Walker and Stuart 1983), as implemented by WinGX (Farrugia, 2012)
No. of measured and independent reflections	1266, 1266
Data completeness to 29.02°θ	100.0%
Indices range of h, k, l	-13 ≤ h ≤ 12, 0 ≤ k ≤ 24, 0 ≤ l ≤ 7
Refinement	
Refinement	Full-matrix least-squares on F ²
Number of reflections, restraints	1266, 0
R ₁ [I > 2σ(I)], R ₁ (all)	0.0277, 0.0351
wR ₂ [I > 2σ(I)], wR ₂ (all)	0.0688, 0.0715
GoF	1.072
No. of refined parameters	116
Δρ _{max} , Δρ _{min} (e ⁻ Å ⁻³)	0.462, -0.795

ellipsoids of atoms located at this cavity is related to the difficulties in accurately modelling the electron density of this site.

Relationship with other species

Ferro-ferri-katophorite belongs to the sodium–calcium amphibole group. In particular, species bearing the katophorite root name fulfil the conditions: ^A(Na+K+2Ca) > 0.5 apfu and 0.5 apfu < ^C(Al+Fe³⁺+2Ti) < 1.5 apfu.

Table 5. Atom coordinates and displacement parameters (Å²).

	x/a	y/b	z/c	U _{eq}	U ¹¹	U ¹³	U ²³	U ²²	U ³³	U ¹²
T1	0.2806(1)	0.0859(1)	0.2984(1)	0.011(1)	0.011(1)	0.001(1)	0.000(1)	0.010(1)	0.011(1)	-0.001(1)
T2	0.2905(1)	0.1719(1)	0.8076(1)	0.011(1)	0.011(1)	0.002(1)	0.000(1)	0.011(1)	0.010(1)	-0.001(1)
M(1)	0	0.0880(1)	½	0.014(1)	0.013(1)	0.003(1)	0	0.018(1)	0.010(1)	0
M(2)	0	0.1800(1)	0	0.010(1)	0.010(1)	0.002(1)	0	0.010(1)	0.011(1)	0
M(3)	0	0	0	0.011(1)	0.013(1)	0.002(1)	0	0.008(1)	0.010(1)	0
M(4)	0	0.2813(2)	½	0.014(1)	0.017(1)	0.009(1)	0	0.010(1)	0.018(1)	0
M(4')	0	0.2713(6)	½	0.014(1)	0.017(1)	0.009(1)	0	0.010(1)	0.018(1)	0
A(m)	0.0443(14)	½	0.085(2)	0.055(3)	0.084(9)	0.079(7)	0	0.022(4)	0.091(7)	0
A2	0	0.4778(1)	0	0.072(6)	0.041(9)	0.059(10)	0	0.058(12)	0.137(18)	0
O1	0.1080(1)	0.0901(1)	0.2143(3)	0.014(1)	0.013(1)	0.002(1)	-0.001(1)	0.016(1)	0.013(1)	-0.001(1)
O2	0.1202(1)	0.1730(1)	0.7326(3)	0.014(1)	0.012(1)	0.002(1)	0.000(1)	0.016(1)	0.014(1)	0.000(1)
O3	0.1096(2)	0	0.7088(4)	0.017(1)	0.014(1)	0.003(1)	0	0.020(1)	0.015(1)	0
O4	0.3661(1)	0.2496(1)	0.7941(3)	0.016(1)	0.018(1)	0.005(1)	-0.001(1)	0.014(1)	0.017(1)	-0.004(1)
O5	0.3497(1)	0.1350(1)	0.0964(3)	0.019(1)	0.015(1)	0.003(1)	0.007(1)	0.024(1)	0.018(1)	0.000(1)
O6	0.3436(1)	0.1185(1)	0.5979(3)	0.018(1)	0.016(1)	0.004(1)	-0.005(1)	0.018(1)	0.019(1)	0.000(1)
O7	0.3369(2)	0	0.2872(5)	0.020(1)	0.016(1)	0.003(1)	0	0.017(1)	0.026(1)	0
H1	0.232(7)	0	0.81(1)	0.0211						

1Set as 1.2 times the U_{eq} of O3.

Table 6. Selected interatomic distances (in Å).

T(1)–O(1)	1.6428(15)	M(2)–O(1) ×2	2.1073(15)	M(4')–O(2) ×2	2.308(9)
T(1)–O(5)	1.6631(16)	M(2)–O(2) ×2	2.0684(16)	M(4')–O(4) ×2	2.314(3)
T(1)–O(6)	1.6628(18)	M(2)–O(4) ×2	1.9523(15)	M(4')–O(5) ×2	2.836(7)
T(1)–O(7)	1.6510(9)	<M(2)–O>	2.0427	M(4')–O(6) ×2	2.643(9)
<T(1)–O>	1.6549			<M(4')–O>	2.525
		M(3)–O(1) ×4	2.1106(14)		
T(2)–O(2)	1.6195(14)	M(3)–O(3) ×2	2.097(2)	A(m)–O(5) ×2	2.907(5)
T(2)–O(4)	1.5963(15)	<M(3)–O>	2.1061	A(m)–O(6) ×2	2.771(8)
T(2)–O(5)	1.6385(18)			A(m)–O(7) ⁽ⁱ⁾	2.533(10)
T(2)–O(6)	1.6548(16)	M(4)–O(2) ×2	2.450(4)	A(m)–O(7) ⁽ⁱⁱ⁾	2.539(9)
<T(2)–O>	1.6273	M(4)–O(4) ×2	2.3502(19)	<A(m)–O>	2.738
		M(4)–O(5) ×2	2.731(3)		
M(1)–O(1) ×2	2.0615(17)	M(4)–O(6) ×2	2.510(3)	A(2)–O(5) ⁽ⁱⁱⁱ⁾ ×2	2.639(19)
M(1)–O(2) ×2	2.1292(15)	<M(4)–O>	2.510	A(2)–O(5) ⁽ⁱⁱⁱ⁾ ×2	3.30(2)
M(1)–O(3) ×2	2.0752(15)			A(2)–O(6) ×2	2.878(15)
<M(1)–O>	2.0886	O(3)–H	1.16(7)	A(2)–O(7) ×2	2.509(4)
				<A(2)–O>	2.832

Symmetry transformations used to generate equivalent atoms: (i) x-½, y+½, z; (ii) -x+½, -y+½, -z; (iii) -x+½, y+½, -z.

The composition Na(NaCa)(Fe₄²⁺Fe³⁺)(Si₇Al)O₂₂(OH)₂ (currently ferro-ferri-katophorite) was named ferri-katophorite in the classification schemes of Leake (1978) and Leake *et al.* (1997). However, no phase with this composition was ever submitted for formal approval to the IMA–CNMNC.

There are currently 9 species (including the one described in this proposal) that justify the katophorite root name (Table 8). To date only katophorite and ferri-fluoro-katophorite have been formally described as such; the others have the 'Redefined' status, or have been identified by chemical analyses (sometimes complemented by single-crystal structural refinement) in publications, but not further characterised.

The samples described by Brøgger (1894) as katophorite from near Grorud, Oslo (Norway) are strongly zoned, and thus the chemical analysis does not correspond to a single phase. If the formula is calculated on a 23O eq basis, the mineral classifies as ferro-ferri-katophorite, however some significant violations to amphibole stoichiometry (such as ΣA = 1.44 apfu) and the presence of Fe³⁺ in tetrahedral coordination indicate that there are analytical problems.

Ferro-ferri-katophorite has been identified by electron microprobe analysis from four other localities: the Xiangshan pluton,

Table 7. Site populations for ferro-ferri-katophorite.

Site	N	Site populations (apfu)	Site scattering (epfu)		Mean bond length (Å)	
			SREF	EMP	Refined	Calculated
T(1)	4	1.39 Al + 2.61 Si				
T(2)	4	4.00 Si				
M(1)	2	0.750 Mg + 0.318 Ti ⁴⁺ + 0.932 Fe ²⁺	39.97	40.23	2.089	2.089
M(2)	2	0.550 Mg + 0.149 Al + 0.006 V ³⁺ + 0.028 Fe ²⁺ + 1.215 Fe ³⁺ + 0.035 Mn ²⁺ + 0.006 Zn + 0.011 Zr	41.22	42.49	2.043	2.043
M(3)	1	0.275 Mg + 0.049 Al + 0.676 Fe ²⁺	21.86	21.51	2.106	2.105
M(4) + M(4')	2	1.081 Ca + 0.906 Na + 0.013 Mn ²⁺	31.91	31.91		
A(m) + A(2)	1	0.230 K + 0.743 Na + 0.026 □ (vacancy)	12.23	12.54		
O3	2	1.394 (OH) ⁻ + 0.606 O ²⁻				

N: number of equivalent sites in the structural formula. apfu: atoms per formula unit; epfu: electrons per formula unit; SREF: single crystal structural refinement; EMP: electron microprobe.

Table 8. Approved species bearing the katophorite root name.

Name	Composition	Reference
Ferro-fluoro-katophorite	Na(NaCa)(Mg ₄ Fe ³⁺)(Si ₇ Al)O ₂₂ F ₂	Oberti <i>et al.</i> (2019)
Ferro-katophorite	Na(NaCa)(Mg ₄ Fe ³⁺)(Si ₇ Al)O ₂₂ (OH) ₂	Pushcharovskii <i>et al.</i> (2003)
Ferro-ferri-katophorite	Na(NaCa)(Fe ₄ ²⁺ Fe ³⁺)(Si ₇ Al)O ₂₂ (OH) ₂	This proposal
Ferro-katophorite	Na(NaCa)(Fe ₄ ²⁺ Al)(Si ₇ Al)O ₂₂ (OH) ₂	Brøgger (1894), redefined by Hawthorne <i>et al.</i> (2012)
Fluoro-katophorite	Na(NaCa)(Mg ₄ Al)(Si ₇ Al)O ₂₂ F ₂	Hawthorne <i>et al.</i> (1993)
Katophorite	Na(NaCa)(Mg ₄ Al)(Si ₇ Al)O ₂₂ (OH) ₂	Oberti <i>et al.</i> (2015a)
Potassic-ferri-katophorite	K(NaCa)(Mg ₄ Fe ³⁺)(Si ₇ Al)O ₂₂ (OH) ₂	Konopleva <i>et al.</i> (2008), Rezvukhin <i>et al.</i> (2020)
Potassic-ferro-ferri-katophorite	K(NaCa)(Fe ₄ ²⁺ Fe ³⁺)(Si ₇ Al)O ₂₂ (OH) ₂	Currie and van Breemen (1996)
Potassic-fluoro-katophorite	K(NaCa)(Mg ₄ ²⁺ Fe ³⁺)(Si ₇ Al)O ₂₂ F ₂	Mazdab (2003)

Funing Co., Qinhuangdao Prefecture, Hebi Province, China (Zhou *et al.*, 1989); Olenii (or Olenyi) Creek, Mt. Kukisvumchorr, Khibiny Massif, Kola Peninsula, Murmanskaja Oblast', Northern Region, Russia (Pekov and Podlesnyi, 2004); the In den Dellen quarries, Mendig, Mayen-Koblenz district, Rhineland-Palatinate, Germany (Schäfer and Schäfer, 2018); and the Motzfeldt center, Igaliku complex, Kujalleq, Greenland (Schönenberger and Markl, 2008). The Mindat database (www.mindat.org, accessed December 29th 2022) lists two other occurrences of ferro-ferri-katophorite, based on personal communications but for which there are no formal publications: the Abdong (or Aptong) Zr–Nb deposit, Pyonggang-gun, Kangwon Province, North Korea, and the Água de Pau volcano, San Miguel, Azores, Portugal.

Calculation of the Fe³⁺/Fe²⁺ ratio and the oxo component in ferro-ferri-katophorite

Note that when only microprobe chemical data are available, the Fe³⁺ content may be severely underestimated, depending on the normalisation scheme used. When the procedure recommended by Hawthorne *et al.* (2012) is followed, starting with all Fe as Fe²⁺, the Fe³⁺/Fe_{Total} ratio is much lower than that obtained by Mössbauer spectroscopy [0.45 vs. 1.07 Fe³⁺ apfu, or Fe³⁺/(Fe²⁺ + Fe³⁺) = 0.16 vs. 0.38, Table 2, column 2]. Thus, it is likely that some ferro-ferri-katophorite will be misidentified as another related species when the analysis is based only on microprobe data. The situation does not improve much if the empirical formula is calculated based on Σcations = 13 apfu (excluding Ca, Na and K), and then adjusting the Fe²⁺/Fe³⁺ ratio to obtain 46 positive charges (Table 8, column 4). In addition, this neglects the presence of any Fe²⁺, Mn and Mg in the B site.

A better procedure is to assign two O²⁻ atoms (located at the O3 position) per each atom of Ti (Table 2, column 3), following the Ti⁴⁺ + 2O²⁻ → (Mg,Fe,Mn)²⁺ + 2(OH)⁻ substitution (Oberti

et al., 1992). Although this is an oversimplification, as only Ti at the M(1) site is associated with deprotonation, this nevertheless gives a better approximation. When this procedure is applied to the microprobe analysis of this paper (starting with all Fe as FeO), it gives a Fe³⁺/(Fe²⁺ + Fe³⁺) ratio which is equal to the value obtained by Mössbauer spectroscopy. In addition, a small amount of Mn is then assigned to the B site, as also indicated by the single-crystal structural refinement.

As a further check, we applied the equation proposed by Oberti *et al.* (2015b, p. 289), using an M(1)–M(2) distance of 3.133 Å for ferro-ferri-katophorite (as calculated from the structure refinement). We obtained a maximum amount of O at the O3 position equal to 0.59 O²⁻ apfu, in good agreement with the 0.61 O²⁻ apfu value obtained by charge balance (with Mössbauer data) or 0.64 O²⁻ apfu calculated assuming the substitution mentioned above.

Acknowledgements. This research was funded by the grants PICT 2698 (2010), PICT-2017-0619, PIP 112-20200101489-CO and SECyT-UNC proyecto Consolidar 2019-2021. CONICET is gratefully acknowledged for a postdoctoral stay of FC at ICMA B (Spain). Members of the IMA-CNMNC are thanked for their comments. We are grateful to two anonymous reviewers for their constructive comments that improved the manuscript, and to Stuart Mills for the editorial handling. This paper is dedicated to the memory of Carmen Galindo, who first noticed the amphibole with peculiar composition at this locality.

Supplementary material. To view supplementary material for this article, please visit <https://doi.org/10.1180/mgm.2023.2>

Competing interests. The authors declare none.

References

- Biglia H. (2015) *Petrología y geoquímica del complejo de sienitas y carbonatitas de la Sierra de Maz, Provincia de La Rioja*. Degree thesis, National University of Córdoba, Argentina.

- Brogger W.C. (1894) Die Eruptivgesteine des Kristianiagebietes, I. Die Gesteine der Grorudit-Tinguait-Serie. *Videnskabssekrets Skrifter. I. Matematisk-naturv.* **1894**, 27–39.
- Casquet C., Pankhurst R.J., Galindo C., Rapela C., Fanning C.M., Baldo E.G.A., Dahlquist J.A., González-Casado J.M. and Colombo F. (2008a) A deformed alkaline igneous rock-carbonatite complex from the Western Sierras Pampeanas, Argentina: Evidence for late Neoproterozoic opening of the Clymene Ocean? *Precambrian Research*, **165**, 205–220
- Casquet C., Pankhurst R.J., Rapela C.W., Galindo C., Fanning C.M., Chiaradia M., Baldo E.G.A., González-Casado J.M. and Dahlquist J.A. (2008b) The Mesoproterozoic Maz terrane in the Western Sierras Pampeanas, Argentina, equivalent to the Arequipa-Antofalla block of southern Peru? Implications for West Gondwana margin evolution. *Gondwana Research*, **13**, 163–175.
- Colombo F., Rius J., Molins E., Biglia H., Galliski M.Á., Márquez-Zavalía M.F., Baldo E.G.A. and Kriscautzky A. (2016) Ferro-ferri-katophorite, IMA 2016-008. CNMNC Newsletter No. 31, June 2016, page 696. *Mineralogical Magazine*, **80**, 691–697.
- Currie K.L. and van Breemen O. (1996) The origin of rare minerals in the Kipawa syenite complex, western Quebec. *The Canadian Mineralogist*, **34**, 435–451.
- Farrugia L.J. (2012) WinGX and ORTEP for Windows: an update. *Journal of Applied Crystallography*, **45**, 849–854.
- Hawthorne F.C. (1983) The crystal chemistry of amphiboles; the octahedral strip. *The Canadian Mineralogist*, **21**, 227–241.
- Hawthorne, F.C. and Oberti, R. (2007) Amphiboles: crystal chemistry. Pp. 1–54 in: *Amphiboles: Crystal Chemistry, Occurrence, and Health Issues* (F.C. Hawthorne, R. Oberti, G. Della Ventura and A. Mottana, editors). Reviews in Mineralogy and Geochemistry, 67. Mineralogical Society of America and the Geochemical Society, Chantilly, Virginia, USA.
- Hawthorne F.C., Ungaretti L., Oberti R., Bottazzi P. and Czamanske G.K. (1993) Li: An important component in igneous alkali amphiboles. *American Mineralogist*, **78**, 733–745.
- Hawthorne F.C., Ungaretti L. and Oberti R. (1995). Site populations in minerals; terminology and presentation of results of crystal-structure refinement. *The Canadian Mineralogist*, **33**, 907–911.
- Hawthorne F.C., Oberti R. and Sardone N. (1996) Sodium at the A site in clinopyroxenes: The effects of composition on the patterns of order. *The Canadian Mineralogist*, **34**, 577–593.
- Hawthorne F.C., Oberti R., Harlow G.E., Maresch W.V., Martin R.F., Schumacher J.C. and Welch M.D. (2012) IMA report nomenclature of the amphibole supergroup. *American Mineralogist*, **97**, 2031–2048.
- Hjollum J. and Madsen M.B. (2009) *Fit(σ) – A Mössbauer Spectrum Fitting Program*. Cornell University Library, USA, doi:10.13140/RG.2.2.19504.92169
- Konopleva N.G., Ivanyuk G.Y., Pakhomovsky Y.A., Yakovenchuk V.N., Men'shikov Y.P. and Korchak Y.A. (2008) Amphiboles of the Khibiny Alkaline Pluton, Kola Peninsula, Russia. *Geology of Ore Deposits*, **50**, 720–731.
- Leake B.E. (1978) Nomenclature of amphiboles. *American Mineralogist*, **63**, 1023–1052.
- Leake B.E., Woolley A.R., Arps C.E., Birch W.D., Gilbert M.C., Grice J.D., Hawthorne F.C., Kato A., Kisch H.J., Krivovichev V.G., Linthout K., Laird J., Mandarino J., Maresch W.V., Nickel E.H., Rock, N.M.S., Schumacher J.C., Smith D.C., Stephenson N.C.N., Ungaretti L., Whittaker E.J.W. and Youzhi G. (1997) Nomenclature of amphiboles; report of the subcommittee on amphiboles of the International Mineralogical Association, Commission on New Minerals and Mineral Names. *The Canadian Mineralogist*, **35**, 219–246.
- Mazdab F.K. (2003) The diversity and occurrence of potassium-dominant amphiboles. *The Canadian Mineralogist*, **41**, 1329–1344.
- Oberti R. and Ghose S. (1993) Crystal chemistry of a complex Mn-bearing alkali amphibole (“tirodite”) on the verge of exsolution. *European Journal of Mineralogy*, **5**, 1153–1160.
- Oberti R., Ungaretti L., Cannillo E. and Hawthorne F.C. (1992) The behaviour of Ti in amphiboles; I, Four- and six-coordinate Ti in richterite. *European Journal of Mineralogy*, **4**, 425–439.
- Oberti R., Vannucci R., Zanetti A., Tiepolo M. and Brumm R. (2000) A crystal-chemical re-evaluation of amphibole/melt and amphibole/clinopyroxene D_{Ti} values in petrogenetic studies. *American Mineralogist*, **85**, 407–409.
- Oberti R., Boiocchi M., Hawthorne F.C., Ball N. A. and Harlow G.E. (2015a) Katophorite from the Jade Mine Tract, Myanmar: mineral description of a rare (grandfathered) endmember of the amphibole supergroup. *Mineralogical Magazine*, **79**, 355–363.
- Oberti R., Boiocchi M., Hawthorne F.C., Cámara F., Ciriotti M.E. and Berge S.A. (2015b) Ti-rich fluoro-richterite from Kariåsen (Norway): the oxo-component and the use of Ti^{4+} as a proxy. *The Canadian Mineralogist*, **53**, 285–294.
- Oberti R., Boiocchi M., Hawthorne F.C., Ball N.A. and Martin R.F. (2019) Ferri-fluoro-katophorite from Bear Lake diggings, Bancroft area, Ontario, Canada: a new species of amphibole, ideally $Na(NaCa)(Mg_4Fe^{3+})(Si_7Al)O_{22}F_2$. *Mineralogical Magazine*, **83**, 413–417.
- Pekov I.V. and Podlesnyi A.S. (2004) Kukisvumchorr Deposit: Mineralogy of Alkaline Pegmatites and Hydrothermalites. *Mineralogical Almanac*, vol. 7, 140 pages + xxiv photo's pages.
- Pushcharovskii D.Yu., Lebedeva Yu.S., Pekov I.V., Ferraris G., Novakova A.A. and Ivaldi G. (2003) Crystal Structure of Magnesioferrikatophorite. *Crystallography Reports*, **48**, 16–23.
- Rezvukhin D.I., Alifirova T.A., Golovin A.V. and Korsakov A.V. (2020) A plethora of epigenetic minerals reveals a multistage metasomatic overprint of a mantle orthopyroxenite from the Udachnaya Kimberlite. *Minerals*, **10**, 264.
- Rodríguez-Carvajal J. (2001) Recent developments of the program FULLPROF. Commission on Powder Diffraction (IUCr). *Newsletter*, **26**, 12–19.
- Schäfer C., and Schäfer H. (2018) Über Dawsonit, Britholith, Ferriallanit und Einige Amphibole aus den Auswürflingen des Laacher Vulkans. *Der Aufschluss*, **69**, 201–2019.
- Schönenberger J. and Markl G. (2008) The magmatic and fluid evolution of the Motzfeldt intrusion in South Greenland: insights into the formation of agpaitic and miaskitic rocks. *Journal of Petrology*, **49**, 1549–1577.
- Shannon R.D. (1976) Revised effective ionic radii and systematic studies of interatomic distances in halides and chalcogenides. *Acta Crystallographica*, **A32**, 751–767.
- Sheldrick G.M. (2008) A short history of SHELX. *Acta Crystallographica*, **A64**, 112–122.
- Walker N. and Stuart D. (1983) An empirical method for correcting diffractometer data for absorption effects. *Acta Crystallographica*, **A39**, 158–166.
- Zhou L., Li, D., Zhao Z. and Wang Y. (1989) Blue asbestos in miarolitic cavities of Xiangshan alkali granite. *Acta Mineralogica Sinica*, **9**, 3.